ISSN: 2639-0108

Research Article

Advances in Theoretical & Computational Physics

Investigation of Conductance and Capacitance of Mesoscopic and Molecular Scale Systems

Afam Uzorka[1]*, Ademola Olatide Olaniyan[1] and Mustaqeem Khan[2]

[1]*Kampala International University, Uganda*

[2]*Interaction Technology Laboratory, Department of Software, Sejong University, Seoul 05006, Korea*

***Corresponding Author**
Afam Uzorka, Kampala International University, Uganda.

Submitted: 2024, Feb 27; **Accepted:** 2024, Mar 24; **Published:** 2024, Apr 11

Citation: Uzorka, A., Olaniyan, A. O., Khan, M. (2024). Investigation of Conductance and Capacitance of Mesoscopic and Molecular Scale Systems. *Adv Theo Comp Phy, 7*(2), 01-15.

Abstract

In addition to a fundamental scientific interest, there has been a significant technological need to build and understand small-scale devices in order to maintain the current rate of progress in increasing computer performance. In this paper, we have discussed the modifications that must be made to the concepts of conductance and capacitance, if they are to be applicable to mesoscopic and molecular scale conductors. We have also reviewed the linear response capacitance theory of Bu ̈ttiker, which can be used to determine the capacitance of a mesoscopic capacitor in a realistic geometry. In order to study capacitance and current at finite bias accurately in a molecular system, we must go beyond the linear response theory. The computational difficulties of determining the charge distribution in non-equilibrium can be resolved by the use of Green's functions which we have reviewed. The system Hamiltonian can in turn be determined accurately by the methods of Density Functional Theory, which we have also outlined.

Keywords: Mesoscopic, Nanoscale, Molecular Scale, Conductance, Capacitance.

1. Introduction

The last two decades saw major progress in experimental control and theoretical understanding of *mesoscopic* and molecular scale electronic devices. This effort is driven by fundamental science interest, due to various new and fascinating quantum phenomena encountered in these systems. There is also the expectation and desire to use advances made towards developing useful applications within the emerging area of nanotechnology, especially in the field of nanoscale electronic computation [1, 2, 3]. In that field there is considerable technological urgency to develop a new device paradigm in order that the current rate of increasing computing performance is maintained [4, 5]. The device technology based on classical and semi-classical physics will be inadequate within a decade if chip components shrink, as projected, to size 20 nm and below. In such a nanoscale, an approach based on quantum physics will be increasingly indispensable.

From the fundamental physics point of view, it has long been of great interest to understand at what length scale and in what manner macroscopic transport laws would start to break down due to quantum effects. Experimental answers to these questions had to wait until sufficient progress has been achieved in fabrication and measurement of small conductors. The experimental effort to study these effects can be roughly divided into investigations of two families of devices, *mesoscopic* and molecular (or nanoscale). Historically, the first to appear were *mesoscopic* devices, first studied in the early 1980's. These systems are intermediate between macro and micro scale (hence mesoscopic) and typically range between 100 nm and 1 pm in size. They consist of many atoms, yet are prepared in such a way that some subset of their electrons maintains quantum coherence over distances of hundreds of nanometers, giving rise to quantum transport behavior. The outstanding system here is the two-dimensional electron gas (2DEG), a carefully manufactured system in which a small subset of total electrons is trapped in a layer at a heterojunction between two semiconducting materials. The electrons in this layer can move over very long distances (over 1μm) without undergoing significant scattering, leading to quantum transport behavior. Metal gates can be applied to the 2DEG in order to "etch" various device structures within it. The study of *mesoscopic* devices is now highly advanced, and a remarkable degree of control over the behavior of electrons in the *mesoscopic* system is possible [6, 7]. In the past decade molecular scale (or nanoscale) devices have been achieved, in which key components may shrink down all the way to one molecule, so that the device size is between 1 nm and 100 nm. In molecular scale, manufacture and control of devices have been harder, as it is difficult to manipulate individual molecules. Nevertheless, the advances have been remarkable, with many fascinating materials such as nanotubes emerging to be used in working devices. Electrical transport studies of carbon nanotubes have yielded

data supporting the possibility of nanotubes functioning as field-effect transistors [8, 9], intramolecular metal-semiconductor diodes [10, 11], and intermolecular-crossed nanotube-nanotube diodes [12, 13]. Nanotubes could be ideal building blocks for nanoelectronics, because they can function both as devices and as wires that access them.

The basic charge transport properties are described by conductance and capacitance. The first measures DC current, the second is necessary for determining current in the AC regime. The Landauer-Bu ̈ttiker formalism [14, 15] is the basic tool for understanding quantum DC conductance ($G = I/V$) in phase-coherent systems with weak electron-electron interaction. In this formalism, the device is attached to leads which are connected adiabatically to macroscopic reservoirs. The conductance is given simply by the probability that an electron will be transmitted from one lead to another across the device. This probability can be obtained, once the Hamiltonian of the system is determined, by solving the Schrodinger equation for the open device configuration and obtaining the scattering wavefunctions. For a low bias voltage, the equilibrium solution is sufficient to obtain the conductance. In classical systems, capacitance is defined as $C = Q/V$ describes accumulation of charge Q in response to a change in the electrostatic potential V in the conductor. In *mesoscopic* and nanoscale systems, this concept of capacitance is generally not valid, as the conductor is generally not at equipotential and hence V is not well defined. A new concept, the electrochemical capacitance, has to be used [16], where $C = eQ/\Delta\mu$ is defined in terms of the electrochemical potential variation Δμ in the macroscopic reservoirs. While for a classical system C is determined only by conductor geometry, the electrochemical capacitance must be found from electron dynamics, by determining the charge rearrangement in the device self-consistently when electrochemical potential Δμ in the reservoirs is varied. A linear response scattering theory developed by Bu ̈ttiker [17, 18, 19] provides the method to calculate electrochemical C to first order using the equilibrium density of states in the device. More generally, some of the most useful transport features are contained in the current-voltage and nonequilibrium charge-voltage characteristics:

$$I_\alpha = I_\alpha[\{V_\beta\}] = \sum_\beta G_{\alpha\beta} V_\beta + \sum_{\beta\gamma} G_{\alpha\beta\gamma} V_\beta V_\gamma + \cdots \quad (1)$$

$$Q_\alpha = Q_\alpha[\{V_\beta\}] = \sum_\beta C_{\alpha\beta} V_\beta + \sum_{\beta\gamma} C_{\alpha\beta\gamma} V_\beta V_\gamma + \cdots \quad (2)$$

Here V_β is the external bias voltage applied at the lead (reservoir) labelled by β. $G_{\alpha\beta}\ V_\beta$ is the linear conductance from lead β to α; $G_{\alpha\beta\gamma}$ is the first order nonlinear conductance. Similarly, $C_{\alpha\beta}$ is the linear capacitance coefficient while $C_{\alpha\beta\gamma}$ is the first order nonlinear capacitance coefficient. These coefficients give charge transport properties of a system, and they can be calculated by solving quantum scattering problems.

Mesoscopic 2DEG conductors can often be adequately described by an effective mass Schrodinger equation. In order to solve this equation in 2D for an open system geometry, various methods have been developed [20]. These methods form an essential tool set for studying mesoscopic conductors. We have developed in this work a method for solving the scattering equation based on a development of the time-dependent scattering technique [21, 22]. In this technique a wavepacket, arriving via one of the leads, is propagated through and out of the system, and the time Fourier transform of the packet wavefunction is then used to obtain the stationary state solutions. An explicit second order differencing scheme is used to evolve the wavefunction on a real space grid [24]. Our method offers many advantages as it treats the boundary conditions efficiently, can handle any lead geometry, and is able to incorporate a uniform magnetic field in the system. Experiments have already shown that the concept of electrochemical capacitance of mesoscopic conductors is important [24, 25, 26], and that capacitance can display non-classical variations as a function of the applied magnetic field [27]. Hence it is important to develop theoretical methods which can model capacitance for these realistic situations. In this work, we will study a mesoscopic capacitor consisting of a multiprobe 2DEG conductor plate capacitively coupled to a classical metal plate.

In order to obtain quantum capacitance for atomic scale devices at a finite bias, the charge variation in response to a small bias can be calculated directly. To do this we have used the formalism of non-equilibrium Green's functions, which we review briefly. We also review the principles of Density Functional Theory, which was essential to modeling molecular scale devices.

2. Landauer-BU ̈ttiker Formalism

In a bulk metallic conductor, the resistance between two contacts is related to bulk conductivity and the dimensions of the conductor, through Ohm's law given by

$$R = \frac{L}{\sigma A} \quad (3)$$

Where σ is the conductivity of the bulk material, L is the length, and A is the cross-sectional area of the conductor. As demonstrated by many experiments in the past two decades, as conductor size is decreased, the resistance may no longer follow Ohm's law. The most striking demonstration of this was the observation of the quantization of conductance by Bagraev, *et al.* [28] (where conductance G=1/R). It was observed that as the width of the conductor is varied, the conductance did not change linearly in L but instead varied in steps of $2\ e^2/h$.

A conductor is usually expected to show non-ohmic behavior if its dimensions are not much larger than certain characteristic lengths. These lengths are:

- λ_F. de Broglie wave length at the Fermi energy, of Fermi

wavelength, as only states near Fermi level carry current. If λ_F is comparable to device size, quantum interference inside device becomes important.

- L_m. Mean free path, it is the average distance an electron travels before its initial momentum is destroyed. This occurs through collisions with impurities, phonons and other electrons. In general, any deviation from perfect crystallinity of the atomic lattice leads to scattering which destroys initial electron momentum.
- L_ϕ. Phase-relaxation length, it is the average distance an electron travels before its initial phase is destroyed. The loss of phase information is caused by inelastic collisions with scatterers such as phonons, other electrons, or impurities with internal degrees of freedom. Rigid scatterers such as crystal imperfections do not contribute to loss of phase.

The conductor is in the "ballistic" regime if its size $L \ll L_m$ and $L \ll L_\phi$. In this case, on average electron flows through the conductor without experiencing collisions of any kind. Even if some imperfection is introduced in the ideal conductor to create a scattering region, the conductor can be considered ballistic. This is true when scattering is due to time-independent changes in potential, and not due to inelastic or dephasing effects. In the ballistic regime, where electrons only interact with static potential and maintains phase coherence, the one-electron Schro ̈dinger equation with some effective potential is often adequate-to adequate transport.

We now proceed to discuss how conductance and current are obtained within the Landauer-Bu ̈ttiker formalism. Fist, we take the case of a perfect ideal conductor connected to two reservoirs, as shown in Figure 1 (a). The large reservoirs are assumed to be at equilibrium and hence have a well-defined electrochemical potential (or equivalently Fermi energy in this case).

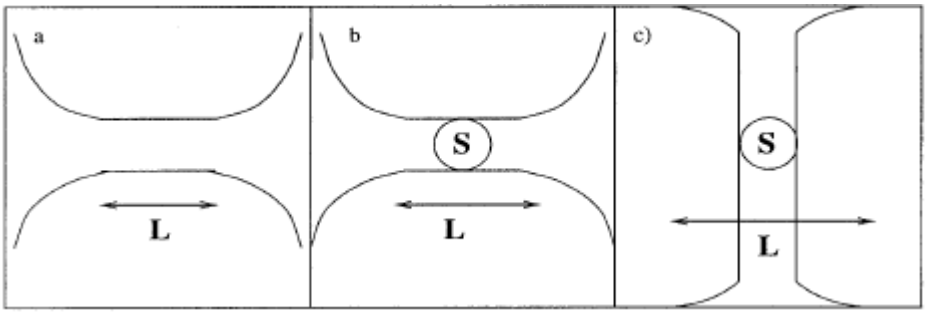

Figure 1: Conductor configurations in the ballistic regime.

We assume that the ideal conductor is made up of repeated 1D crystalline unit cell Length□ L□_c. We also assume that electrons are described by one-electron effective potential with no magnetic field. Thus the boundaries of the conductor are defined by the wall of potential well in which the electrons are confined. The ideal conductors are assumed to fan out smoothly (adiabatically) joining to the large reservoir in such a way that an electron exiting the ideal conductor has no probability of scattering back at the junction. Hence electrochemical potential in the reservoirs determines the population of states of the ideal conductor from the reservoirs and hence their energy distribution is governed by that of the reservoirs. The ideal conductor is assumed to be ballistic, and all inelastic scattering is assumed to take place inside the reservoirs.

The propagating wave functions of such an ideal conductor are Bloch states defined, for each real k in the Brillouin zone, in the standard form

$$\psi_{kn}(r) = u_{kn}(x,y,z)e^{ikz} \tag{4}$$

With energy of each state denoted as $E_n(k)$, z is the propagation direction along the conductor, and u the periodic function satisfying $u_{kn}(x,y,z) = u_{kn}(x,y,z+L_c)$. The propagation direction of each state is given by the sign of its group velocity $u_{kn} = dE_n(k)/dk$, with positive v indicating propagation in the +z direction. The number of states (or modes) propagating in the +z and –z direction is equal. Thus we can define the function M(E), which gives the number of modes present at energy E propagating in the +z(or –z) direction.

Now the occupation of +z propagating modes is described by $f^+(E)$, and those in –z direction as $f^-(E)$ where for adiabatic contacts the distribution functions f^+ and f^- will just be the distribution functions of right and left reservoirs respectively. A uniform 1D electron gas with n electrons per unit length moving with a velocity v carries a current of env. As the electron density of a single k-state is $(1/L_c)$, we write the current I^+ carried by +v states as

$$I^+ = \frac{e}{L_c}\sum_{kn}^{+} u_{kn} f^+\big(E_n(k)\big) = \frac{e}{L_c}\sum_{kn}^{+} \frac{1}{\hbar}\frac{\partial E_n(k)}{\partial k} f^+(E_n(k)) \tag{5}$$

Where the sum is over Bloch states with positive v. Converting the sum over k to an integral

$$\sum_k \rightarrow 2 \times \frac{L_c}{2\pi}\int dk \tag{6}$$

where factor 2 is for spin degeneracy, we obtain

$$I^{+} = \frac{2e}{h}\int_{-\infty}^{+\infty} f^{+}(E)M(E)dE \tag{7}$$

where the function M(E) is the number of propagating modes at energy E. Now, if we work at zero temperature, and we impose a bias voltage which gives different electrochemical potentials μ_1 and μ_2 for two reservoirs, we can combine I^{+} and I^{-} to obtain

$$I = \frac{2e^2}{h}M\frac{\mu_1 - \mu_2}{e} = \frac{2e^2}{h}M(V_1 - V_2) \tag{8}$$

where we have assumed the number of modes M to be a constant in the energy range $\mu_1<E<\mu_2$. We thus obtain conductance

$$G = \frac{2e^2}{h}M \tag{9}$$

Because M is an integer, G is "quantized".

Equivalently, the resistance is given by

$$G^{-1} \equiv \frac{(\mu_1 - \mu_2)/e}{I} = \frac{h}{2e^2M} \approx \frac{12.9k\Omega}{M} \tag{10}$$

We note that, even though the conductor is ideal and there is no electron scattering inside it, there is considerable finite resistance. This resistance is the contact resistance as it arises from the interface between the ideal quantum conductor with only a few modes and a contact which has infinitely many transverses modes. Another justification for this interpretation is the fact that for the ideal conductor the voltage drop must occur at the contacts.

We now consider what happens when the ideal conductor is modified by the presence of a finite region S that contains deviations from the ideal potential profile, as shown in Figure 1 (b). Electrons moving through the conductor can now undergo scattering at the imperfections in S. The scattering is assumed to be caused by some time independent deviation of the crystal potential landscape, and not by inelastic or dephasing collisions. Thus an electron entering the conductor via mode *i* will have some probability T_i of passing through the conductor, and probability R_i = 1-T_i of scattering and reflecting back. Here we assumed that there is no magnetic field in the system and hence these probabilities are the same for electrons entering from either contact. In this case we can use an argument similar to those used for deriving Eq.9 and obtain

$$G = \frac{2e^2}{h}\sum_{i=1}^{M} T_i = \frac{2e^2}{h}MT \tag{11}$$

where T is the average probability that an electron injected at one end of the conductor will transmit to the other end. This relation is known as the Landauer formula [29].

The Landauer formula can be extended to cases where the scattering region is connected to more than two ideal conductors. In this case it is easier to think of the scattering region S as connected via a number of ideal leads to external reservoirs. Now an electron entering the system through mode i of lead β will scatter and exit the system through contact *α*. The product of the number of modes of lead *β* and the mode average of the probability of exiting through lead α, is defined as $T_{\alpha\leftarrow\beta}$.

Through a generalization of the two lead situation, the current in terminal α is

$$I_\alpha = \frac{2e}{h}\sum_{\beta}\left[T_{\beta\leftarrow\alpha}\mu_\alpha - T_{\alpha\leftarrow\beta}\mu_\beta\right] = \sum_{q}\left[G_{\beta\alpha}V_\alpha - G_{\alpha\beta}V_\beta\right] \tag{12}$$

Where we have defined conductance matrix

$$G_{\alpha\beta} \equiv \frac{2e^2}{h}T_{\alpha\leftarrow\beta} \equiv \frac{2e^2}{h}T_{\alpha\beta} \tag{13}$$

The modification for the multiprobe case was due to Bu¨ttiker [30], and formula (13) is known as Landauer- Bu¨ttiker formula [31].

One can obtain the transmission probabilities $T_{\alpha\beta}$ from the scattering wave functions obtained by solving the Schro¨dinger equation for the open system. A scattering wave function can be constructed so that in the leads it is a superposition of one incoming mode in the incoming lead and all outgoing modes in all leads. Choosing unit amplitude and zero phase in the incoming mode j in lead α as $s_{\alpha i,\beta j}$. This defines the complex scattering matrix $s_{\alpha\beta}$ with dimensions given by the number of modes in lead α and β. The matrices can be combined into a global scattering matrix S which can then be used to relate the incoming and the outgoing amplitudes and phases. The conductances are obtained from the scattering matrix through:

$$G_{\alpha\beta} \equiv \frac{2e^2}{h} Tr(s^{+}_{\alpha\beta} s_{\alpha\beta} \equiv \frac{2e^2}{h} T_{\alpha\beta} \tag{14}$$

So far in this discussion we have focused on a situation where the scattering region S is connected to narrow leads with a finite number of modes (Figure 1(a,b)). However, the ideas discussed here can be easily extended to the limit where the leads become large and states there become continuous in energy (Figure 1(c)). This geometry is applicable to the very important case of a molecule or a nanowire connecting two bulk surfaces, as is the case in many experiments. Here the sum over modes is expanded to run over all incoming states of semi-infinite surface.

The conductance defined so far only governs the current for a small applied bias (linear regime). For a two probe device, a straightforward generalization of the current expression for finite bias and temperature is given by [32]

$$I = \frac{2e^2}{h} \int_{-\infty}^{+\infty} T(E)\,[f_L(E) - f_R(E)]dE \tag{15}$$

where T(E) is the total transmission probability through all modes. Here the Fermi distribution functions are given as

$$f_{(L,R)} = \frac{1}{e^{\beta(E-\mu_{(L,R)})} + 1} \tag{16}$$

where $\beta = 1/k_B T$) and μ_L and μ_R are the electrochemical potentials in the left and right lead. For zero temperature, the Fermi function becomes a step function, and the integration range of Eq.(15) reduces to the window between the lead electrochemical potentials. We have to keep in mind that for a finite bias the transmission T(E) is a function of the bias.

3. Classical and Quantum Capacitance

We have just discussed how the concept of resistance changes once we go to small scale. A similar reformulation must be performed for the concept of capacitance. Classically, capacitance is a concept which applies to a system of conductors. Following a standard argument of classical electrostats, a metallic conductor can have no electric field in its interior, and hence the electrostatic potential within it is constant and the entire volume of a given i-th conductor is at equipotential V_i. Any free charge on the conductor arranges itself into an infinitesimally thin sheet on the surface of the conductor, in such a way that the equipotential condition within the conductor interior is satisfied. For small V_i, the total charge Q_i on a given conductor is then linearly related to the potential of all conductors of the system,

$$Q_i = \sum_j C_{ij} V_j \tag{17}$$

where C_{ij} are the capacitance coefficients. While the above definition holds for isolated conductors, a typical system has the conductors connected to the outside world, which imposes V_i onto the conductors. Then the capacitance coefficients C_{ij} describe how much charge enters the conductors in response to a variation of applied bias. Classically, capacitance is purely a geometric quantity, i.e. it depends only on the shape and spatial arrangements of the conductors (and dielectrics). Determining capacitance coefficients C_{ij} requires solving the Poisson equation with appropriate boundary conditions on conductor surfaces, which can be quite involved but for which software packages exist.

The key assumption of the classical theory requires well defined conductors, with zero electric field inside. This cannot be true on the small scale as the electric field cannot be discontinuous in space. The electric field penetrates into the conductor to a depth which is on the order of the screening length of the material. The screening length can also be thought of as the length over which the electric field of a point test charge introduced into the system would be cancelled out by the rearrangement of free electrons [33]. The screening length depends on electron dynamics and is material dependent.

In bulk metals the screening length is small, of the order of 1Å, therefore the notion of classical capacitance is valid as long as conductor dimensions are greater than that length scale. Similarly, many microscopic systems are still well described by a classical capacitance [34]. However, in a number of conductors of lower dimensionality, such as nanotubes and two-dimensional electron gases, the screening length can frequently be comparable to system dimensions [16]. In such systems, it no longer makes sense to use the concept of conductor potential V_i, as the system is not at equipotential. Hence a new definition

of capacitance at this length scale is required. The concept of capacitance has to be modified to that of *electrochemical* capacitance, where the conductor is connected to an electron reservoir with an electrochemical potential μ. Then we can look at change in accumulated charge dQ in response to the variation Δμ relative to some reference potential.

$$\Delta Q_i = \sum_j C_{ij} e \Delta V_j \tag{18}$$

Furthermore, in contrast to the classical case, there is no reason for the charge accumulation to be linear in voltage at finite bias, and hence in order to make sense the capacitance coefficients have to be considered functions of applied bias, as in Eq.(2). As there is no longer an equipotential surface, geometric techniques are no longer applicable. Instead, one has to actually calculate the change in electron dynamics in response to change of external electrochemical potential. From these, one can calculate the change in the amount of charge present in a conductor, and hence the amount of charge that has entered the system from the reservoir. The needs to consider electron dynamics make quantum capacitance intimately related to quantum transport.

The fall description of electron dynamics in small scale structures is obviously a great challenge. Therefore, in order to make progress in our study of capacitance, we must make approximations, and restrict our studies to systems which are reasonably described by the approximations. Below we proceed to outline what can be considered as the next step beyond classical capacitance: the scattering theory of linear quantum, capacitance of Bu¨ttiker [19].

4. Scattering Theory for Quantum Capacitance

We have described the study of transport through the scattering approach, where one uses scattering wave functions and scattering matrices. We continue to apply the scattering approach to electrochemical capacitance, following the approach of Bu¨ttiker [19]. We assume our system to consist of a number of conductors which are quantum coherent, and each is connected to a reservoir with an electrochemical potential. The electrons in the conductors are described by some one-electron effective potential, and they interact via Coulomb interaction treated via one loop RPA approximation [19].

In linear response, we consider how the system responds to an infinitesimal change in the electrochemical potential of the reservoir (which is brought about by applying a bias voltage). The initial electrostatic potential $U([\mu_\alpha],\boldsymbol{r})$is a complicated function of position r as well as the electrochemical potentials μ_α. A small variation in the electrochemical potential brings the system to a new equilibrium state, with potential given by $U([\mu_\alpha + d\mu_\alpha],\boldsymbol{r})$. When $d\mu_\alpha \to 0$, we expand the difference

$$eU([\mu_\alpha + d\mu_\alpha],\boldsymbol{r}) - eU([\mu_\alpha],\boldsymbol{r}) = edU([\mu_\alpha],\boldsymbol{r}) = \sum_\alpha u_\alpha(\boldsymbol{r})\, d\mu_\alpha \tag{19}$$

where $u_\alpha(\boldsymbol{r})$ is called the *characteristic potential,*

$$u_\alpha(\boldsymbol{r}) = e\frac{dU([\mu_\alpha],\boldsymbol{r})}{d\mu_\alpha}\Big|_{d\mu_\alpha=0} \tag{20}$$

The characteristic potential $u_\alpha(\boldsymbol{r})$ has some simple properties. First, deep inside reservoir α, a change in $d\mu$ must induce a change in electrostatic potential $edU = d\mu_\alpha$, because a reservoir is a large metal where perfect screening is assumed. Therefore we conclude that for r inside reservoir α, $u_\alpha = edU/(d\mu_\alpha = 1.)$ Second, since the change of $d\mu_\alpha$, does not affect other reservoirs, we conclude that $u_\alpha = 0$ if r is in reservoir β. Finally, if all μ's are changed by the same constant change we have only moved the energy scale of our system, and this cannot give rise to any change in the electric field (hence dU is constant). This means $\sum_\alpha u_\alpha = 1$ from Eq(19). To summarize, we have

$$u_\alpha(\boldsymbol{r}) = 1 \; if \; \boldsymbol{r} \; inside \; reservoir \; \alpha \tag{21}$$

$$u_\alpha(\boldsymbol{r}) = 0 \; if \; \boldsymbol{r} \; inside \; reservoir \; \beta \tag{22}$$

$$\sum_\alpha u_\alpha = 1 \; for \; all \; \boldsymbol{r} \tag{23}$$

Under the change of electrochemical potential $d\mu_\alpha$ in reservoir α, a charge rearrangement in the system occurs due to two contributions. First, there is the injected charge, given by filling up the density of states for incoming carriers:

$$d\rho_{inj,\alpha}(\boldsymbol{r}) = \frac{dn(\boldsymbol{r},\alpha)}{dE} d\mu_{\boldsymbol{\alpha}} \tag{24}$$

Here the density $dn(\boldsymbol{r},\alpha)/dE$ is the injectivity, which describes the partial density of states associated with carriers arriving at point r from reservoir α after a variation $d\mu_\alpha$. It can be obtained straightforwardly from the scattering wave functions [19].

$$\frac{dn(\boldsymbol{r},\alpha)}{dE} = \sum \frac{|\psi_\alpha^2|}{hv} \tag{25}$$

Where the sum is over all ψ's describing electrons entering the system from reservoir α, v is the group velocity, and h the Planck constant. The sum of injectives from all reservoirs gives the total local density of states:

$$\frac{dn(\boldsymbol{r})}{dE} = \sum_\alpha \frac{dn(\boldsymbol{r},\alpha)}{dE} \tag{26}$$

Second, in response to the injected charge, there is the induced charge density, generated by the charge in the electrostatic potential inside the device. The induced charge density can be described via the Lindhard function [35].

$$d\rho_{ind,\alpha}(\boldsymbol{r}) = \int d\boldsymbol{r}' II(\boldsymbol{r},\boldsymbol{r}') u_\alpha(\boldsymbol{r}') d\mu_\alpha \tag{27}$$

The analytical expression for the Lindhard function is difficult to obtain, therefore Bu¨ttiker uses the Thomas-Fermi approximation [19]. In this approximation, the induced density is locally related to the potential.

$$d\rho_{ind,\alpha}(\boldsymbol{r}) = -\sum_\alpha \frac{dn(\alpha,\boldsymbol{r})}{dE} edU(\boldsymbol{r}) = -\frac{dn(\boldsymbol{r})}{dE} u_\alpha(\boldsymbol{r}) d\mu_\alpha \tag{28}$$

Here the density $dn(\alpha,\boldsymbol{r})/dE$ is the emissivity, which described the partial density of states associated with carriers ejected into reservoir α from point r upon variation of the potential at point r. The sum of the emissivities for all α gives the total local density of states. In zero magnetic field, the emissivity is equal to the injectivity, and in nonzero magnetic field B they are connected by a useful relation [36, 37]

$$\frac{dn(\alpha,\boldsymbol{r},\boldsymbol{B})}{dE} = \frac{dn(\boldsymbol{r},\alpha,-\boldsymbol{B})}{dE} \tag{29}$$

In Thomas-Fermi approximation, the Lindhard function becomes local:

$$\mathrm{II}_{TF}(\boldsymbol{r},\boldsymbol{r}') = \delta(\boldsymbol{r}-\boldsymbol{r}') \frac{dn(\boldsymbol{r})}{dE} \tag{30}$$

The characteristic potential is then obtained self-consistency by solving the Poisson equation

$$-\nabla^2 u_\alpha(\boldsymbol{r}) + 4\pi^2 \frac{dn(\boldsymbol{r})}{dE} u_\alpha(\boldsymbol{r}) = 4\pi^2 \frac{dn(\boldsymbol{r},\alpha)}{dE} \tag{31}$$

This equation is easily obtained from the Poissoin equation for the electrostatic potential U®. Once the characteristic potential is known, the sum of injected and induced charge integrated over the volume of the conductor can be determined. This gives the accumulation of charge dQ_α on conductor α due to the electrochemical potential change in reservoir β, from which we obtain the capacitance matrix coefficients

$$C_{\alpha\beta} = \frac{edQ_\alpha}{d\mu_\beta} = e^2 \int_{\Omega_\alpha} d^3r \left[\delta_{\alpha\beta} \frac{dn(\boldsymbol{r},\alpha)}{dE} - \frac{dn(\alpha,\boldsymbol{r})}{dE} u_\beta(\boldsymbol{r})\right]. \tag{32}$$

To give an example, we consider the case of a parallel plate capacitor. As usual, we ignore the edge effects, and cast the Poisson equation in 1D. First, we consider the case illustrated in Figure 2(a) where two conductors are separated by distance d, conductor 1 extends for $x < 0$, and conductor 2 for $x > d$. As the conductors are separated and carries at any point can arrive and

leave from only one reservoir, the injectivity is equal to the total density of states, and the injectivity is equal to the emissivity. The injectivities $dn(r,1)/dE$ and $dn(r,2)/dE$ are taken to have uniform value dn/dE inside their conductors and zero outside, where for simplicity the same density dn/dE in conductors 1 and 2 is assumed. The total density of states is equal to dn/dE inside the conductors and is zero for $0 < x < d$. Here the screening length is defined as $\lambda^{-2} = (4\pi e^2\ dn)/dE$. The 1D Poisson equation of 31 is solved for these assumptions and we obtain the capacitance matrix elements $C_{11} = C_{22} = -C_{21} = -C_{21} = C$, with

$$\frac{C}{A} = \frac{1}{4\pi(d + 2\lambda)} \tag{33}$$

We see that for large $d \gg \lambda$ the capacitance is classical, but when d becomes comparable to λ there is a quantum correction. This correction to capacitance has been observed experimentally [16, 38]. The capacitance saturates to a constant value $A/(8\pi\lambda)$ as separation $d \rightarrow 0$ and does not diverge as in the classical case. The reason for this is clear from looking at the potential $u(x)$ and the charge distribution $d\rho(x)$ (Figure 2). When d becomes comparable to screening length, the classical assumption that all charge is located in an infinitesimally thin sheet on the surface and that all potential drops outside the conductors does not describe the situation correctly. The charge and potential drop over the distance on the order of the screening length λ, leading to a reduction of capacitance relative to classical value.

In real quantum systems the wavefunctions will start to overlap as conductors approach each other, leading to electron transport and a breakdown of the simple capacitance model. There is an exception to his however, in the case where the wavefunctions in the two conductors have different symmetry properties, so that the integrated overlap between them is zero and no DC transport is possible.

We now consider the case where wavefunctions of the two capacitor plates have a finite overlap, but no DC transport takes place. The absence of DC transport implies that even though the densities associated with the two conductors do overlap in some region of space, they can still be viewed as if they were spatially separated conductors.

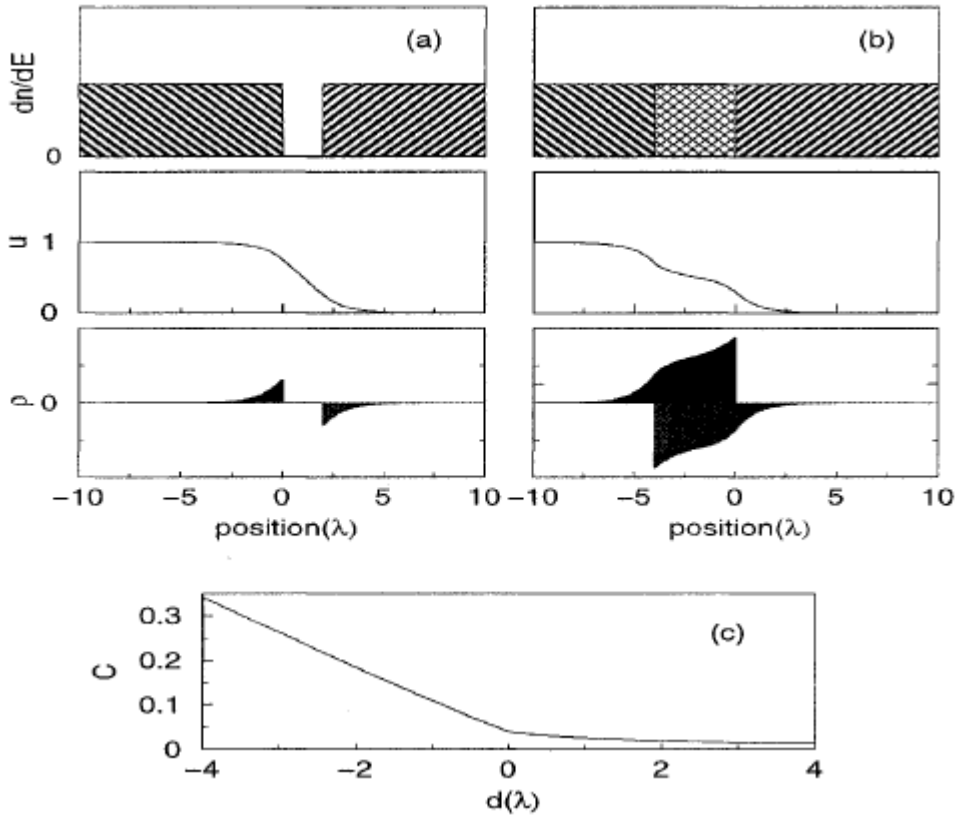

Figure 2: The injectivities dn/dE (x), characteristic potential $u(x)$, and accumulated charge $\rho(x)$ are shown in (a) and (b) for finite separation d=1 and inter-penetration d=4 respectively. Charge arriving from the left reservoir is black and from the right red. The capacitance as a function of separation (positive) and inter-penetration (negative) d is shown in (c).

Hence the injectivity and the emissivity for each conductor are the same, i.e. $dn(\alpha,\boldsymbol{r})/dE = dn(\boldsymbol{r},\alpha)/dE$. One can usefully think of this configuration as one conductor penetrating into the other, as illustrated in Figure 2(b). We assume that the two wavefunctions, and hence the injectiveities, overlap over some distance d. Thus $dn(\boldsymbol{r},1)/dE = dn/dE$ extends for $x<0$, and $dn(\boldsymbol{r},2)/dE = dn/dE$ for $x>-d$, with the overlap occurring for $-d<x<0$, where again uniform densities of states are assumed. The total density of states in the

screening term will be dn/dE everywhere except in the overlap region, where it will be a combination of injectivities from both reservoirs; thus in the overlap it will have the value $2\times dn/dE$, where dn/dE here indicates the single conductor density of states. As there is no DC transport, any electron which arrives at a point r from a given reservoir must exit the system into the same reservoir. With these assumptions, half of the induced charge in the overlap region will be emitted into each reservoir. We can solve the Poisson equation again with the terms just described, with details provided in appendix A. we obtain the characteristic potentials and the charge distribution, and we integrate over charges associated with reservoir 1 and 2. This gives

$$\frac{C}{A} = \frac{(1+e^{-d/\lambda})}{4\sqrt{2\pi}\lambda\left(\left(\sqrt{2}+1\right)+e^{-d/\lambda}\left(\sqrt{2}-1\right)\right)} + \frac{d}{4\pi\lambda^2} \tag{34}$$

We see that there is a term linear in d which causes a steep linear increase in capacitance for increasing insertion depth. The capacitance C as a function of distance d, obtained from equations (33) and (34), is shown in Figure 2 (c). We can see that C increases slowly as the separation distance decreases to zero, and then increases linearly with the insertion distance, which is considered here as negative separation distance. It is clear from the plot that, in this simple model, the overlapping of electron densities in the two conductors causes a large increase in the value of the capacitance. The plot of charge densities for the inter-penetration case shows that the positive and negative charges are partially located in the same region of space, lowering the electrostatic energy, and therefore more charge can be stored for a given applied bias.

5. AC formulation of Capacitance

Now we discuss what happens to the notion of quantum capacitance when the possibility of transport between conductors is allowed, meaning that carriers can flow between reservoirs. In this case it is useful to consider the AC picture, where variations of electrochemical potentials are time-dependent. Now, the main quantity of interest is the admittance, which relates the time-dependent current to the time-dependent voltage. The capacitance as well as conductance will make contributions to admittance.

First, we reconsider the case of isolated conductors under AC bias. In the presence of slowly oscillating potentials $d\mu_\alpha \exp(-iwt)$, our system of conductors is driven through a sequence of equilibrium states given by $U([\mu_\alpha(t)],\boldsymbol{r})$. The quasi-stationary potential distribution away from the reference state is

$$edU(\boldsymbol{r},t) = \sum_\alpha u_\alpha(\boldsymbol{r}) d\mu_\alpha(t) \tag{35}$$

From the relation $dQ_\alpha = \sum_\beta C_{\alpha\beta}(d\mu_\beta/e)$ one obtains leading-order terms of the current and admittance [19]

$$I_\alpha = -iwdQ_\alpha = -w\sum_\beta C_{\alpha\beta}\left(d\mu_\beta(w)/e\right) \tag{36}$$

$$g_{\alpha\beta}(w) = (eI_\alpha(w))/d\mu_\beta(w) = -iwC_{\alpha\beta} \tag{37}$$

Next, if we expand the discussion to allow carrier propagation from reservoir α to reservoir β, the admittance must also contain a DC component. To first order in w, we will have [19]

$$g_{\alpha\beta}(w) = g_{\alpha\beta}(0) - iwE_{\alpha\beta} + O(w^2) \tag{38}$$

where $E_{\alpha\beta}$ is the emittance and $g_{\alpha\beta}(0)$ the DC conductance. The first order capacitative properties of the system can now be described by the emittance matrix $\{E_{\alpha\beta}\}$. The emittance is given, within Thomas-Fermi approximation, by [19]

$$E_{\alpha\beta} = e^2\int d\boldsymbol{r}^3 \frac{dn(\alpha,\boldsymbol{r},\beta)}{dE} - e^2\int dr^3 \frac{dn(\alpha,\boldsymbol{r})}{dE} u_\beta(\boldsymbol{r}) \tag{39}$$

This expression is obtained through an argument similar to that used to obtain $C_{\alpha\beta}$ in Eq.(32). The difference is that instead of using injectivity, one has to use a modified density of states to allow for the possibility of carriers moving between α and β. To define the new partial density, we consider a small oscillation in electrochemical potential μ_β that injects into the system a charge density $e(dn(r,\beta)/dE)\, d\mu_\beta$. A fraction of the carriers which reach point r will eventually reach contact α. The density of these carriers is the partial density of states$(dn(\alpha,r,\beta)/dE)$. Clearly, in the case of no transport between α and β, this density is zero, and we have $E_{\alpha\beta} = C_{\alpha\beta}$. Thus some entries of the emittance matrix can be thought as capacitance coefficients [39].

Using a Green's functions argument, it can be shown [40] that the density of states in the above expression can be related to the scattering matrix through.

$$\frac{dn(\alpha,\boldsymbol{r},\beta)}{dE} = -\frac{1}{4\pi i} Tr\left(s^{+}_{\alpha\beta}\frac{\delta s_{\alpha\beta}}{e\delta U(\boldsymbol{r})} - \frac{\delta s^{+}_{\alpha\beta}}{e\delta U(\boldsymbol{r})} s_{\alpha\beta}\right) \tag{40}$$

$$\frac{dn(\alpha,\boldsymbol{r})}{dE} = -\frac{1}{4\pi i}\sum_{\beta} Tr\left(s^{+}_{\alpha\beta}\frac{\delta s_{\alpha\beta}}{e\delta U(\boldsymbol{r})} - s_{\alpha\beta}\frac{\delta s^{+}_{\alpha\beta}}{e\delta U(\boldsymbol{r})}\right) = \sum_{\beta}\frac{dn(\alpha,\boldsymbol{r},\beta)}{dE} \tag{41}$$

These quantities are rather difficult to calculate due to the presence of the functional derivative. They have been calculated only for some simple systems where analytical or efficient computational means could be employed [38]. However we have here demonstrated that certain elements of the emittance matrix can be reduced to capacitance coefficients, and some of these can be determined from injectivities only. This discussion illustrates that calculating capacitance properties of a system with zero conductance is much easier computationally than studying a general system where DC conductance is non zero.

6. Capacitance under finite bias

Various efforts have been made to go beyond linear response in scattering approach. Some of the approaches involved calculating higher order coefficients in the expansion of capacitance in voltage [41] or frequency [42]. However, the general finite bias dependence of capacitance can only be calculated through determining the full charge density self-consistency. This can be accomplished within scattering theory, by determining the scattering the scattering wave functions and hence the injectyivities, and then the electron density in the system.

$$\rho(\boldsymbol{r}) = \int_{-\infty}^{\infty} dE \sum_{\beta} f_{\beta}(E)\frac{dn(\boldsymbol{r},\beta)}{dE} \tag{42}$$

where f_{β} is the Fermi distribution in the reservoirs under finite bias. The effective potential generated by $\rho(\boldsymbol{r})$ would could then be determined by an appropriate method and then used to obtain injectivities, until self-consistency was achieved. One could proceed to vary electrochemical potentials in the distribution functions, determine $\rho(\boldsymbol{r})$ before and after variation, and from this obtain dQ and determine capacitive response of the system for any bias. This has been done previously for simple systems [43]. To do this accurately for real nanoscale structure requires a considerable effort. There are many difficulties, in particular using the scattering wavefunctions to determine the charge density is a large computational problem. Once the charge density is obtained, the effective potential for the electrons must be determined accurately.

We will introduce the tools that will allow us to accurately model transport and capacitance in nanoscale devices. First, we briefly introduce equilibrium and non-equilibrium Green's functions, which will offer us the ability to calculate charge density very efficiently. Then we will give an overview of density functional theory, which will allow us to determine the effective potential for the electrons for a given charge density accurately.

7. Green's functions approach

In order to study molecular scale devices in an open system geometry, we must have an efficient method to determine their charge density. While scattering theory is a good point of departure for determining conductance, the scattering states cannot be used to construct the density in an efficient way. Instead, we require the capabilities offered by the Green's function formalism to accomplish this task. The Green's function is a widely tool in mathematics and physics. Broadly speaking, in our context the Green's function gives the response at any point (inside or outside the conductors) due to an excitation at any other. If there appropriate Green's function of the system is known, then practically all important information about the system can be obtained from it. The retarded Green's function G^{R}, of a Hamiltonian H, at every E, is defined by the relation:

$$G^{R}(E) = \big((i\eta)I - H\big)^{-1}, \eta \to 0. \tag{43}$$

If H describes an open system connected to finite reservoirs, then the matrix requiring inversion to obtain G^{R} is infinite and cannot be inverted directly. However, if we can divide the system into some central region C and lead regions L, then we can think of the G^{R} as:

$$\begin{bmatrix} G_L & G_{LC} \\ G_{CL} & G_C \end{bmatrix} = \begin{bmatrix} \big((E+i\eta)I - H_L\big) & H_{LC} \\ H_{CL} & (EI - H_C) \end{bmatrix}^{-1} \tag{44}$$

Here, H_L,H_C is the sub-Hamiltonian matrix describing the lead and the central regions; H_CL,H_LC describe the coupling between these regions.

Now we are able to write G in the form

$$G_C = EI - H_C - \sum_L \tag{45}$$

Where

$$\sum_L = H_{CL} G_L H_{LC} \tag{46}$$

It is advantageous to rewrite G in this way because if G_L can be determined for the lead, then we only need to determine the finite matrix G_C.

The total density of states of the system is given by the imaginary part of the Green's function. Hence in equilibrium, assuming all states are filled up to some energy, the electron density in the system can be obtained as:

$$\hat{\rho} = \int_{-\infty}^{\mu} Re[G^R] \tag{47}$$

Transport properties can also be determined from the Green's functions of the system. The Fisher-Lee relation [44] for zero bias conductance, here defined for multi-lead case, gives conductance from lead β to lead α as:

$$G_{\alpha\beta} = \frac{2e^2}{h} Tr\left[\Gamma_\alpha G_C \Gamma_\beta G_C^+\right] \tag{48}$$

Where the coupling matrix Γ as

$$\Gamma_L = i[\sum_L - \sum_L^+] \tag{49}$$

This Fisher-Lee relation demonstrates the equivalence between the Green's function and the scattering matrix formalisms.

Under a finite bias which drives current flow, the system is in non-equilibrium, so one must use Keldysh nonequilibrium Green's functions (NEGF) [15, 45, 46]. In this approach, we consider the system as coupled to reservoirs with some distribution f. Through coupling to reservoirs described by a quantity $\sum^<$, electrons enter the system. The essential non-equilibrium function is $G^<$ which contains information about the particle distribution in the system. It is related to G^R and G^A through the Keldysh equation [46].

$$G^< = G^R(E) \sum^<(E) G^A(E) \tag{50}$$

Where, in a mean field theory,

$$\sum^<(E) = \sum_\beta 2 f_\beta(E) Im\left[\sum_\beta(E)\right] \tag{51}$$

The $G^<$ can be used to determine the density as

$$\hat{\rho} = \int_{-\infty}^{\mu} Re[G^<] \tag{52}$$

This can be thought of as a density obtained by adding contributions of electron waves entering the device contacts.

8. Density Functional Theory

To study transport properties of molecular devices, we need a method which can model the microscopic degrees of freedom accurately and efficiently. Here we briefly outline the principles of Density Functional Theory (DFT) which lies at the heart of the modern electronic theory. The basis for DFT is the fact that the non-degenerate ground state energy for a system of N interacting electrons, E_N, is a unique functional of the single-particle density $\rho(r)$:

$$E_N = E_N[\rho(\boldsymbol{r})] \tag{53}$$

Since all properties are determined by the ground-state density, any system can be studied by minimizing a unique, universal total energy functional $E[\rho]$. Thus the motivating result of DFT is that the complicated problem of obtaining the ground state for an interacting system of electrons is reduced to minimizing the functional $E[\rho]$. The central problem of DFT is to determine the form of this functional. Unfortunately, the exact form is not known, but one can construct approximations to it which give excellent results. The standard method for doing this begins by formally writing

$$E[\rho] = T[\rho] + \frac{1}{2}\int d\boldsymbol{r}d\boldsymbol{r}'\frac{\rho(\boldsymbol{r})\rho(\boldsymbol{r}')}{|\boldsymbol{r}-\boldsymbol{r}'|} + \int d\boldsymbol{r}\rho(\boldsymbol{r})V_{ext}(\boldsymbol{r}) + E_{XC}[\rho] \tag{54}$$

where the kinetic energy contribution is $T[\rho]$, and the next two terms represent mean-field interaction energy and the energy due to the external potential V_{ext}, respectively. All non-classical corrections and many-body effects not included in the first three terms are described by the exchange-correlation functional $E_{XC}[\rho]$. Practical calculations use one of many standard approximate forms for $E_{XC}[\rho]$. One of these forms is given by Local Density Approximation (LDA), and is calculated for the high and low-density limits of the homogeneous electron gas and interpolated in between as a function of ρ. The LDA which we have used to obtain DFT results in this work is based on the parameterization suggested by Falletta et al. [47].

Many applications of DFT are based on the Kohn-Sham (KS) equation [48]. In this approach the density is constructed from non-interacting electron functions ψ^i:

$$\rho(\boldsymbol{r}) = \sum_i \left(\psi^i(\boldsymbol{r})\right) * \psi^i(\boldsymbol{r}) \tag{55}$$

Where $\psi^i|\psi^j\rangle = \delta_{ij}$. The Kohn-Sham Kinetic energy is given by

$$T_{KS} = \sum_{i=1}^{N}\langle\psi^i|\frac{-\nabla^2}{2}|\psi^i\rangle \tag{56}$$

The true kinetic energy $T[\rho]$ does not equal the KS kinetic energy T_{KS}, but the difference can be absorbed into a redefined correlation functional. In the ground state, the variation of the total energy is stationary with respect to the wavefunctions $\{\psi^i(r)\}$

$$\frac{\delta[\rho]}{\delta\psi^i(r')} = 0 \tag{57}$$

The orthogonality conditions are maintained by introducing the Lagrange multipliers E_{ij}:

$$\frac{\delta[\rho]}{\delta\psi^i(r')} - E^{ij}\psi^j = 0 \tag{58}$$

which gives, after diagonalizing E_{ij},

$$[-\frac{\nabla^2}{2} + \int d\boldsymbol{r}'\frac{\rho(\boldsymbol{r}')}{|\boldsymbol{r}-\boldsymbol{r}'|} + V_{ext}(\boldsymbol{r}) + V_{ion-el}(\boldsymbol{r}) + V_{XC}\big(\rho(\boldsymbol{r})\big)]\psi^i(\boldsymbol{r}) = E^i\psi^i(\boldsymbol{r}) \tag{59}$$

where V_{XC} is the exchange-correlation potential:

$$V_{XC}[\rho] \equiv \frac{\delta E_{XC}[\rho]}{\delta\rho(\boldsymbol{r})} \tag{60}$$

We have also formally separated the ion-electron potential from the total external potential acting on the electrons. This equation reduces the interacting problem to a set of non-interacting Schrödinger-like equations. Since the equation (59) depends on the solutions $\{\psi^i\}$ through the density $\rho(\boldsymbol{r})$, it is a non-linear self-consistent eigen value problem which requires a considerable amount of computational effort to solve. We now discuss some of the techniques used to make the solution of this problem computationally feasible.

We start by recasting Eq.(59) into a more convenient form.

$$V_H(\boldsymbol{r}) = \int d\boldsymbol{r}'\frac{\rho(\boldsymbol{r})}{|\boldsymbol{r}-\boldsymbol{r}'|} \tag{61}$$

The Hartree potential and the $V_{ion\text{-}et}$ potential go as N/R and –N/R at large separation R and hence are long ranged potentials which may be troublesome to work with. By adding and subtracting neutral charge density $\rho^{NA}(\boldsymbol{r})$ with the property

$$\int dr\rho^{NA}(\boldsymbol{r} - R_{\boldsymbol{I}}) = Z_I \tag{62}$$

We rewrite Eq.(59) as

$$H = -\frac{\nabla^2}{2} + \sum_J V^{NA,J}(\boldsymbol{r} - \boldsymbol{R_J}) + V_{\delta H}(\boldsymbol{r}) + V_{XC}(\boldsymbol{r}) + V_{ext}(\boldsymbol{r}) \tag{63}$$

Where

$$\nabla^2 V_{\delta H}(\boldsymbol{r}) = 4\pi[\rho(\boldsymbol{r}) - \sum_J \rho^{NA}(\boldsymbol{r} - \boldsymbol{R_J})] = 4\pi\rho_{\delta H}(\boldsymbol{r}) \tag{64}$$

And

$$\mathrm{V}^{NA}(\boldsymbol{r}) = \sum_J V^{NA,J}(\boldsymbol{r} - \boldsymbol{R}_J) = \sum_J \left[V^J_{ion-et}(\boldsymbol{r} - \boldsymbol{R_J}) + \int d\boldsymbol{r}' \frac{\rho^{NA,J}(\boldsymbol{r}' - \boldsymbol{R_J})}{|\boldsymbol{r} - \boldsymbol{r}'|}\right] \tag{65}$$

Now $V^{NA}(\boldsymbol{r})$ and $V_{\delta H}$ are short ranged potentials more convenient to work with numerical.

To avoid solving all-electron problem, it is possible to replace $V_{ion-et}(\boldsymbol{r})$ with a pseudopotential to describe valence electrons only [49]. For this pseudopotential to depict valence electrons accurately, it must in general be nonlocal and angular momentum dependent:

$$V_{NL} = \sum_l |l > V_l < l| \tag{66}$$

One particularly useful formulation of the pseudopotential which we use, due to Kleinman and Bylander (KB) [50], introduces a separable form for nonlocal pseudopotential, using spherical harmonics Y_{lm},

$$V_{KB}(\boldsymbol{r}, \boldsymbol{r}') = \sum_{lm} |Y_{lm}(\Omega_r) W_l(r) > \epsilon_l < W_l(r') Y_{lm}(\Omega_r)|$$

$$W_l(r) \equiv V_l \psi_l(r) \tag{67}$$

$$\epsilon_l \equiv \frac{\langle \psi_l | V_l(r) | \psi_l \rangle}{\langle \psi_l | V_l^2(r) | \psi_l \rangle}$$

which is easier to calculate.

Once the Kohn-Sahn Hamiltonian Eq. 63 is well defined, in order to solve it numerically one must employ a set of basis functions in order to represent the electronic wavefunction. Many different types of basis sets are possible, offering various combinations of speed, accuracy and ease of implementation. In widely used plane wave methods, the wave functions are expanded in terms of plane waves, giving a high accuracy at relatively large computational cost. The reason for this is the need to include a large number of plane waves to model the system accurately. Also this method is restricted to periodic boundary conditions, and thus it is unable to study transport with finite bias. In contrast, real space basis sets expand the wavefunctions in term of basis functions localized in real space. The real space basis we use in this work is a modified Linear Combination of Atomic Orbitals (LCAO) minimal basis, one obtains a reasonable accuracy, much faster numerics and the ability to model large non-periodic systems with transport. The accuracy of the LCAO basis can be progressively improved by adding higher momentum atomic orbitals to the basis set.

9. Conclusion

We provided an overview of the Landauer-Bu¨ttiker formalism for conductance in ballistic quantum coherent conductors, and discuss how it differs from the classical result. Then we discuss the Bu¨ttiker formalism for calculating capacitance for quantum coherent conductors, and contrast it with the classical approach to capacitance. In order to obtain quantum capacitance for atomic scale devices at a finite bias, the charge variation in response to a small bias can be calculated directly. To do this we have used the formalism of non-equilibrium Green's functions, which we reviewed briefly. We also review the principles of Density Functional Theory, which was essential to modeling molecular scale devices.

10. Conflict of Interest

The authors declare there is no conflict of interest

11. Data availability: Not applicable

References

1. Gajewicz, A., Rasulev, B., Dinadayalane, T. C., Urbaszek, P., Puzyn, T., Leszczynska, D., & Leszczynski, J. (2012). Advancing risk assessment of engineered nanomaterials: application of computational approaches. *Advanced drug delivery reviews, 64*(15), 1663-1693.
2. Matteucci, F., Giannantonio, R., Calabi, F., Agostiano, A., Gigli, G., & Rossi, M. (2018, July). Deployment and exploitation of nanotechnology nanomaterials and nanomedicine. In *AIP conference proceedings* (Vol. 1990, No. 1). AIP Publishing.
3. DeLuca, M., Shi, Z., Castro, C. E., & Arya, G. (2020). Dynamic DNA nanotechnology: toward functional nanoscale devices. *Nanoscale Horizons, 5*(2), 182-201.
4. Morawska, L., Thai, P. K., Liu, X., Asumadu-Sakyi, A., Ayoko, G., Bartonova, A., ... & Williams, R. (2018). Applications of low-cost sensing technologies for air quality monitoring and exposure assessment: How far have they gone?. *Environment international, 116*, 286-299.
5. Callaghan, C. W. (2018). Surviving a technological future: Technological proliferation and modes of discovery. *Futures, 104,* 100-116.
6. Roccapriore, K. M., Huang, N., Oxley, M. P., Sharma, V., Taylor, T., Acharya, S., ... & Kalinin, S. V. (2022). Electron-beam induced emergence of mesoscopic ordering in layered MnPS3. *ACS nano, 16*(10), 16713-16723.
7. Shi, C., Hu, F., Wu, R., Xu, Z., Shao, G., Yu, R., & Liu, X. Y. (2021). New silk road: from mesoscopic reconstruction/functionalization to flexible meso-electronics/photonics based on cocoon silk materials. *Advanced Materials, 33*(50), 2005910.
8. Scuratti, F., Salazar-Rios, J. M., Luzio, A., Kowalski, S., Allard, S., Jung, S., ... & Caironi, M. (2021). Charge transport in high-mobility field-effect transistors based on inkjet printed random networks of polymer wrapped single-walled carbon nanotubes. *Advanced Functional Materials, 31*(5), 2006895.
9. Blaudeck, T., Preuß, A., Scharf, S., Notz, S., Kossmann, A., Hartmann, S., ... & Schulz, S. E. (2019). Photosensitive Field-Effect Transistors Made from Semiconducting Carbon Nanotubes and Non-Covalently Attached Gold Nanoparticles. *physica status solidi (a), 216*(19), 1900030.
10. Shanmugam, N. R., & Prasad, S. (2018). Characteristics of Carbon Nanotubes for Nanoelectronic Device Applications. *Nanopackaging: Nanotechnologies and Electronics Packaging*, 597-628.
11. Saraç, Y., Şener, S. Ş., Baltakesmez, A., Güzeldir, B., & Sağlam, M. (2020). A comparative study on theoretical and experimental methods using basic electrical parameters of Au/CNTs/lnP/Au–Ge diodes. *Journal of Alloys and Compounds, 824,* 153899.
12. Zhang, L., Dai, X., Li, T., Li, J., & Li, H. (2018). CH3NH3PbX3 (X= I, Br) encapsulated in silicon carbide/carbon nanotube as advanced diodes. *Scientific Reports, 8*(1), 15187.
13. Peng, R., Pan, Y., Liu, B., Li, Z., Pan, P., Zhang, S., ... & Liu, X. (2021). Understanding Carbon Nanotube-Based Ionic Diodes: Design and Mechanism. *Small, 17*(31), 2100383.
14. Yasuda, K., Mogi, M., Yoshimi, R., Tsukazaki, A., Takahashi, K. S., Kawasaki, M., ... & Tokura, Y. (2017). Quantized chiral edge conduction on domain walls of a magnetic topological insulator. *Science, 358*(6368), 1311-1314.
15. Wulf, U. (2020). A one-dimensional effective model for nanotransistors in Landauer–Büttiker formalism. *Micromachines, 11*(4), 359.
16. Janissek, A., Lenz, J., Giudice, F. D., Gaulke, M., Pyatkov, F., Dehm, S., ... & Weitz, R. T. (2021). Ionic liquid gating of single-walled carbon nanotube devices with ultra-short channel length down to 10 nm. *Applied Physics Letters, 118*(6).
17. Büttiker, M., Thomas, H., & Prêtre, A. (1993). Mesoscopic capacitors. *Physics Letters A, 180*(4-5), 364-369.
18. Bueno, P. R. (2018). Common principles of molecular electronics and nanoscale electrochemistry.
19. He, J., Yue, X., & Guo, H. (2020). Mesoscopic capacitance oscillations due to quantum dynamic coherence in an interacting quantum capacitor. *Applied Physics Letters, 117*(11).
20. Kotilahti, J. (2021). *Quantum interference in dynamically driven mesoscopic conductors* (Master's thesis).
21. Goings, J. J., Lestrange, P. J., & Li, X. (2018). Real-time time-dependent electronic structure theory. *Wiley Interdisciplinary Reviews: Computational Molecular Science, 8*(1), e1341.
22. Coccia, E., Assaraf, R., Luppi, E., & Toulouse, J. (2017). Ab initio lifetime correction to scattering states for time-dependent electronic-structure calculations with incomplete basis sets. *The Journal of Chemical Physics, 147*(1).
23. Dinh, P. M., Vincendon, M., Coppens, F., Suraud, E., & Reinhard, P. G. (2022). Quantum Dissipative Dynamics (QDD): A real-time real-space approach to far-off-equilibrium dynamics in finite electron systems. *Computer Physics Communications, 270*, 108155.
24. Belhboub, A., Simon, P., & Merlet, C. (2019). On the development of an original mesoscopic model to predict the capacitive properties of carbon-carbon supercapacitors. *Electrochimica Acta, 327,* 135022.
25. Liu, W., He, J., Guo, H., & Gao, J. (2018). Electrochemical capacitance modulation in an interacting mesoscopic capacitor induced by internal charge transfer. *Physical Review B, 97*(16), 165420.
26. Lopes, L. C., Santos, A., & Bueno, P. R. (2021). Measuring quantum conductance and capacitance of graphene using impedance-derived capacitance spectroscopy. *Carbon, 184*, 821-827.
27. Amico, L., Basko, D. M., Bergeret, S., Buisson, O., Courtois, H., Fazio, R., ... & Schön, G. (2018). Mesoscopic electron transport and atomic gases, a review of Frank WJ Hekking's scientific work. *SciPost Physics, 5*(1), 009.
28. Bagraev, N. T., Grigoryev, V. Y., Klyachkin, L. E., Malyarenko, A. M., Mashkov, V. A., Romanov, V. V., & Rul, N. I. (2017). High-temperature quantum kinetic effect in silicon nanosandwiches. *Low Temperature Physics, 43*(1), 110-119.
29. Sowa, J. K., Lambert, N., Seideman, T., & Gauger, E. M. (2020). Beyond Marcus theory and the Landauer–Büttiker approach in molecular junctions. II. A self-consistent Born

approach. *The Journal of Chemical Physics, 152*(6).
30. Esfarjani, K. (2021). Theory of Non-equilibrium Heat transport in anharmonic multiprobe systems at high temperatures. *Entropy, 23*(12), 1630.
31. Yu, Y., Zhang, Y. Y., Liu, L., Wang, S. S., Guan, J. H., Xia, Y., & Li, S. S. (2020). Chebyshev polynomial method to Landauer–Büttiker formula of quantum transport in nanostructures. *AIP Advances, 10*(7).
32. Tien, N. T., Phuc, V. T., & Ahuja, R. (2018). Tuning electronic transport properties of zigzag graphene nanoribbons with silicon doping and phosphorus passivation. *AIP Advances, 8*(8).
33. Ciftja, O., Livingston, V., & Thomas, E. (2017). Cyclotron motion of a charged particle with anisotropic mass. *American Journal of Physics, 85*(5), 359-363.
34. Härtel, A. (2017). Structure of electric double layers in capacitive systems and to what extent (classical) density functional theory describes it. *Journal of Physics: Condensed Matter, 29*(42), 423002.
35. Zhu, X., Guo, J., Zhang, J., & Plummer, E. W. (2017). Misconceptions associated with the origin of charge density waves. *Advances in Physics: X, 2*(3), 622-640.
36. Deo, P. S. (2021). *Mesoscopic route to time travel. S*pringer.
37. Reiss, H. (2019). Radiative transfer, non-transparency, stability against quench in superconductors and their correlations. *Journal of Superconductivity and Novel Magnetism, 32*(6), 1529-1569.
38. Sreenath, V., & George, B. (2018). An improved closed-loop switched capacitor capacitance-to-frequency converter and its evaluation. *IEEE Transactions on Instrumentation and Measurement, 67*(5), 1028-1035.
39. Leleu, S., Rives, B., Caussé, N., & Pébère, N. (2019). Corrosion rate determination of rare-earth Mg alloys in a Na2SO4 solution by electrochemical measurements and inductive coupled plasma-optical emission spectroscopy. *Journal of Magnesium and Alloys, 7*(1), 47-57.
40. Morales-García, Á., Valero, R., & Illas, F. (2017). An empirical, yet practical way to predict the band gap in solids by using density functional band structure calculations. *The Journal of Physical Chemistry C, 121*(34), 18862-18866.
41. Scarborough, C., & Grbic, A. (2020). Accelerated N-path network analysis using the floquet scattering matrix method. *IEEE Transactions on Microwave Theory and Techniques, 68*(4), 1248-1259.
42. Kuchařík, J., & Němec, H. (2021). Strong confinement-induced nonlinear terahertz response in semiconductor nanostructures revealed by Monte Carlo calculations. *Physical Review B, 103*(20), 205426.
43. Ågren, H., Harczuk, I., & Vahtras, O. (2019). Decomposition of molecular properties. *Physical Chemistry Chemical Physics, 21*(5), 2251-2270.
44. Pitié, S., Seydou, M., Dappe, Y., Martin, P., Maurel, F., & Lacroix, J. C. (2021). Fast Fisher-Lee approach for conductance calculations on BTB-based molecular junctions: effects of isomerization and electrode coupling. *arXiv preprint arXiv:2107.08836*.
45. Lima, L. R., & Lewenkopf, C. (2022). Local equilibrium charge and spin currents in two-dimensional topological systems. *Physical Review B, 105*(8), 085420.
46. Rahman, H., & Kleinekathöfer, U. (2018). Non-equilibrium Green's function transport theory for molecular junctions with general molecule-lead coupling and temperatures. *The Journal of Chemical Physics, 149*(23).
47. Falletta, S., Wiktor, J., & Pasquarello, A. (2020). Finite-size corrections of defect energy levels involving ionic polarization. *Physical Review B, 102*(4), 041115.
48. Gomez Pueyo, A., Marques, M. A., Rubio, A., & Castro, A. (2018). Propagators for the time-dependent Kohn–Sham equations: Multistep, Runge–Kutta, exponential Runge–Kutta, and commutator free Magnus methods. *Journal of chemical theory and computation, 14*(6), 3040-3052.
49. Chen, Y., Ma, J., & Li, W. (2019). Understanding the thermal conductivity and Lorenz number in tungsten from first principles. *Physical Review B, 99*(2), 020305.
50. Kim, T. Y., Ferretti, A., & Park, C. H. (2018). Effects of spin-orbit coupling on the optical response of a material. *Physical Review B, 98*(24), 245410.